RESEARCH ARTICLE | MAGNETISM AND MAGNETIC MATERIALS | FEBRUARY 27 2017

Study of switching behavior of exchange-coupled nanomagnets by transverse magnetization metrology

Himadri S. Dey; Gyorgy Csaba ; Gary H. Bernstein; Wolfgang Porod

AIP Advances 7, 056321 (2017)
https://doi.org/10.1063/1.4977721
CHORUS

Study of switching behavior of exchange-coupled nanomagnets by transverse magnetization metrology

Himadri S. Dey,[a] Gyorgy Csaba, Gary H. Bernstein, and Wolfgang Porod
Center for Nano Science and Technology, Notre Dame, Indiana 46556, USA

(Presented 1 November 2016; received 23 September 2016; accepted 22 November 2016; published online 27 February 2017)

We investigate the static switching modes of nanomagnets patterned from antiferromagnetically exchange-coupled magnetic multilayers, and compare them to nanomagnets having only dipole coupling between the ferromagnetic layers. Vibrating sample magnetometry experiments, supported by micromagnetic simulations, reveal two distinct switching mechanisms between the exchange-coupled and only dipole-coupled nanomagnets. The exchange-coupled nanomagnets exhibit gradual switching of the layers, dictated by the strong antiferromagnetic exchange coupling present between the layers. However, the layers of the only dipole-coupled nanomagnets show abrupt nucleation/growth type switching. A comprehensive understanding of the switching modes of such layered and patterned systems can add new insight into the reversal mechanisms of similar systems employed for spintronic and magneto-logic device applications. [http://dx.doi.org/10.1063/1.4977721]

I. INTRODUCTION

Magnetic multilayer systems have a vast range of applications in data storage,[1] sensing,[2] computing,[3] information processing[4] and biomedical applications.[5] Typically, a building block for such systems is composed of two ferromagnetic layers separated by a non-magnetic metal (for spin-valve) or insulator (for tunnel junction). The magnetic properties of these multilayers are markedly different depending on whether they are in the form of thin films or lithographically patterned structures. As they are scaled down below about 100 nm, shape anisotropy and dipole coupling between the magnetic layers start to play a significant role in determining the switching properties. Various experimental tools including vibrating sample magnetometer (VSM),[6–8] alternating gradient magnetometer (AGM),[9,10] superconducting quantum interference device (SQUID),[6] magneto-optic Kerr effect (MOKE)[2] and x-ray scattering[11] have been used to study the reversal mechanisms of such sub-100 nm systems. Reversal of nanomagnets with different size and shape, namely rectangular,[10] elliptical,[8] circular[2] etc. have been discussed in these studies. Here we report the magnetic hard-axis switching properties of a patterned rectangular CoFe/Ru/CoFe nanomagnet system determined using a method we call "transverse magnetization metrology" (TMM),[12,13] which uses the vector coils of a VSM (Microsense EV7) to obtain magnetization information in the direction perpendicular to that of the applied field along with the more-commonly obtained magnetization in the direction of the field. This technique has been previously used, for example, to study the reversal of Fe-Ga nanowires[14] and measure magnetic dipole coupling between adjacent nanomagnets.[12] We extend the scope of this technique to understanding the switching modes of the CoFe layers that are coupled by oscillatory RKKY type interactions, whose coupling, either antiferromagnetic or ferromagnetic, is determined by the thickness of a Ru spacer layer.[15]

[a]Corresponding author: Himadri Dey, email: hdey@nd.edu

We found strong antiferromagnetic exchange coupling for a 0.8 nm Ru layer between two CoFe layers, and only dipole coupling for a 1.2 nm Ru layer.[7] Noting that shape anisotropy and dipole coupling are present in both systems, but exchange coupling is present in only the first, we refer to the multilayer with 0.8 nm Ru as 'exchange-coupled', and the multilayer with 1.2 nm Ru as 'dipole-coupled'. We patterned these multilayers into large arrays of nominally identical rectangular nanomagnets, and measured their magnetic switching using the TMM method, which magnetized the nanomagnets along their hard axes, and simultaneously measured the magnetization along their easy axes. We observed gradual switching of the CoFe layers in the exchange-coupled nanomagnets and abrupt switching in the dipole-coupled nanomagnets, which reveals two markedly different switching modes in the two systems: the dipole-coupled magnets switch by domain nucleation and growth in the nanomagnets while the exchange-coupled system switches by gradually turning single-domain-like states. The experimental observations agree well with micromagnetic simulations. Section II presents the sample preparation and VSM measurements. The micromagnetic simulations are shown in section III. Finally, section IV concludes the paper.

II. EXPERIMENTAL STUDY OF SWITCHING

The CoFe/Ru/CoFe films were sputtered on a Si substrate in presence of Ar in an Oerlikon magnetron sputtering system having a base pressure of approximately 5×10^{-8} mbar. The top and bottom CoFe layers were 10 nm and 3 nm, respectively. A 10 nm Ta seed layer was deposited under the bottom CoFe layer, and a 5 nm Ta capping layer was deposited directly on the top CoFe layer. The strongest antiferromagnetic interlayer exchange coupling was found for approximately 0.8 nm Ru spacer layer thickness, and the magnetic hysteresis of the film, measured by the VSM, is shown in the inset of Fig. 1(a). The magnitude of the antiferromagnetic exchange coupling constant, J, was found to be 5×10^{-4} J/m^2, which is similar to our and other groups' earlier results.[7] The multilayer was patterned into an array of about 10^8 200 × 100 nm^2 nanomagnet stacks separated by 200 nm using a Vistec 5200/5000 100 kV electron beam lithography system. After lithography and development of the resist, we evaporated ~12 nm thick Ti as a hard mask on the sample and lifted it off. Then the excess CoFe outside the Ti mask was etched by Ar milling. Details of the etch process can be found elsewhere.[7] The resulting sample was an ensemble of lithographically patterned nanomagnet stacks. A micrograph of the structures is shown in the inset of Fig. 1(a). We also sputtered multilayers with 1.2 nm Ru (hysteresis of the film shown in the inset of Fig. 1(b)), and patterned it into nanomagnet stacks, keeping the other stack parameters the same. The slightly thicker Ru essentially eliminates the antiferromagnetic exchange coupling ($J \sim 0$), but the dipole coupling between the layers remains approximately the same. All other process conditions were kept the same as those applied for the exchange-coupled nanomagnets.

We used the vector scan coils of the VSM to measure the y-component of the magnetization (M_y) as a magnetic field (H) is applied at 3° from the hard-axis (x) direction. This angle provides a small bias to the magnets along their easy axes. Figures 1(a) and (b) show the experimental M_y vs H_x plots for the exchange-coupled and only dipole-coupled nanomagnets, respectively. In Fig. 1(a), the VSM data show a gradual evolution of M_y for the exchange-coupled nanomagnets as the magnetic field is cycled from -500 mT to +500 mT, and then in the reverse direction. If we consider the M_y vs H_x curve from -500 mT to +500 mT, this gradual evolution indicates that there is no abrupt switching of the layers. The peak of M_y (M_y/M_s = 0.5) appears at H_x = 20 mT, representing the perfectly antiferromagnetically aligned layers at this field. Approximately at H_x = 310 mT, M_y becomes zero.

For the dipole-coupled nanomagnets, in Fig. 1(b), M_y peaks around H_x = 10 mT, where M_y/M_s = 0.58. At H_x = 60 mT, M_y crosses zero. In this case, abrupt switching of the layers can be seen around this field. M_y decreases until H_x = 70 mT, and reaches a minimum value (M_y/M_s = -0.28) before increasing again, approaching zero magnetization. Since the VSM curves show only the net magnetization of the dots, we used micromagnetic simulations to understand the domain configurations during switching.

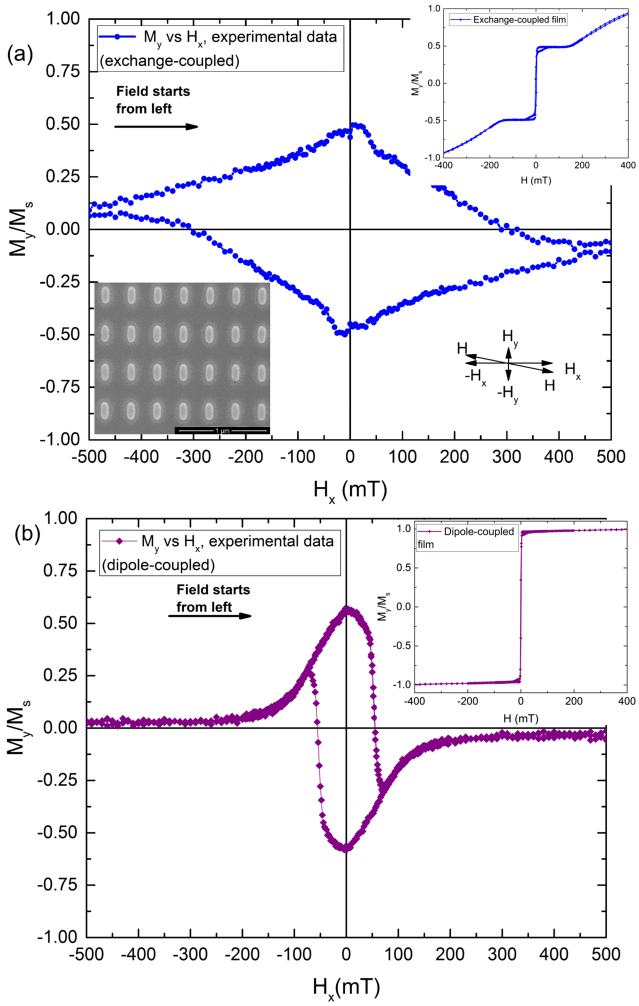

FIG. 1. VSM measurement on the patterned nanomagnet array. (a) Exchange-coupled nanomagnets (b) dipole-coupled nanomagnets.

III. MICROMAGNETIC SIMULATIONS

We used OOMMF[16] to simulate the exchange-coupled and dipole-coupled nanomagnets. A single nanomagnet having a nominal shape of 200 × 100 nm^2 was simulated for both cases. We used the experimentally determined value of antiferromagnetic exchange coupling constant, $J = -5\times10^{-4}$ J/m^2, for the exchange-coupled nanomagnet, and $J = 0$ for the dipole-coupled nanomagnet. We used the 'two-surface exchange' module in OOMMF, and performed the simulations at 0 K, choosing the unit cell size for the simulation to be 5 × 5 × 1 nm^3. For CoFe, we used the following parameter values: saturation magnetization, $M_s = 14\times10^5$ A/m; exchange constant, $A = 30\times10^{-12}$ J/m^2; and damping constant, $\alpha = 0.5$. Just as in the experiments, the field was applied at an angle of 3° from the hard axis (x) direction of the nanomagets, and the y-component of the magnetization (M_y) was plotted against the x-component of the applied field (H_x). Figures 2(a) and (b) show the M_y vs H_x plots for exchange- and dipole-coupled nanomagnets, respectively.

In Fig. 2(a), the net M_y of the two CoFe layers is plotted as the magnetic field is swept from -500 mT to + 500 mT, and then in the reverse direction. Magnetization snapshots corresponding to the top and bottom layers at different H_x are also shown in the figure. Even under a strong field at H_x = - 400 mT (point 'a'), the layers are not fully biased in the direction of H_x, owing to the strong antiferromagnetic exchange coupling and dipole coupling between them. Then H_x is

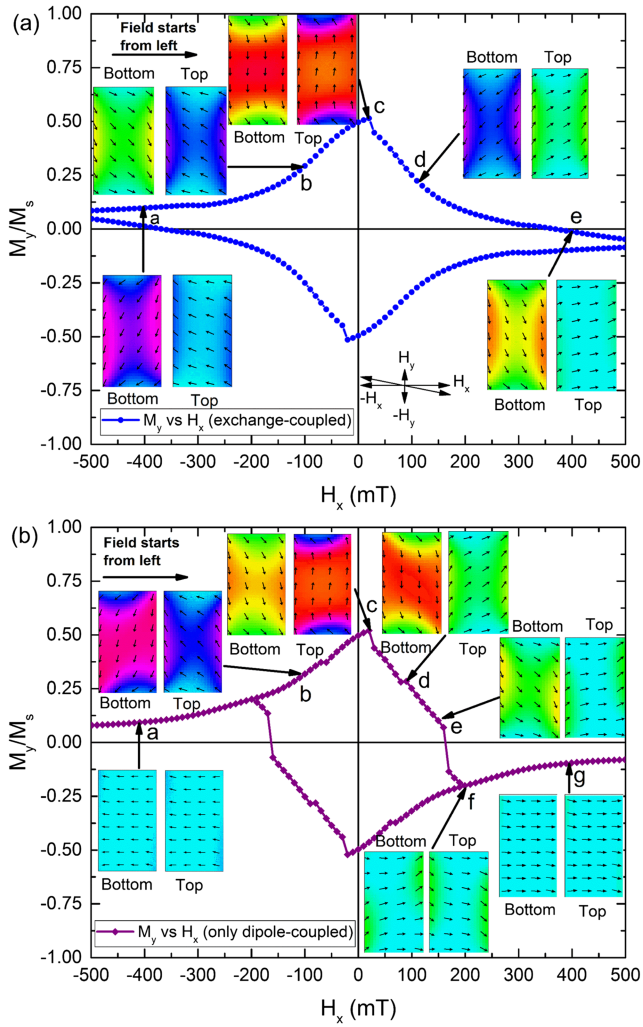

FIG. 2. OOMMF simulations of reversal mechanism for (a) exchange-coupled nanomagnet (b) dipole-coupled nanomagnets.

gradually reduced in magnitude, and when H_x = -100 mT (point 'b'), the strong antiferromagnetic exchange coupling and dipole coupling between the layers, and shape anisotropies of the two layers force them to point antiferromagnetically to each other in a canted domain configuration. As H_x is further reduced, the layers tend to orient themselves more antiferromagnetically and parallel to the y direction. When H_x = + 20 mT (point 'c'), the layers are almost perfectly antiferromagnetically aligned to their easy axis (y) direction. As H_x is further increased, the layers again gradually start rotating together subject to the external field, maintaining their antiferromagnetic alignment due to the strong antiferromagnetic exchange coupling. At H_x = +100 mT (point 'd'), we again see a canted antiferromagnetic alignment as the one observed for H_x = -100 mT, except that the layers are now canted in a different domain orientation. For the rest of the magnetization cycle, the switching of the layers occurs in a gradual manner. A snapshot of layer magnetizations at H_x = +400 mT (point 'e') is also shown. Figures 1(a) and 2(a) indicate a close agreement between the experiment and simulation. Gradual switching of the layers can be fully explained by the simulations. The peaks of the M_y curves appear at H_x = 20 and -20 mT in both the experiment and simulation. The M_y peaks (M_y/M_s = 0.5 and -0.5) also show similar values in the experiment and simulation. M_y becomes zero at approximately H_x = 340 mT and -340 mT, which are close to the experimental values (H_x = 310 mT and -310 mT).

Figure 2(b) shows the simulated magnetization evolution of the layers in the dipole-coupled nanomagnet. In this case, 'J' was set to zero in the simulation, keeping everything else the same. At H_x = -400 mT (point 'a'), the layers are already nearly perfectly biased in the direction of H_x, unlike the

exchange-coupled nanomagnet. Point 'b' represents the situation when the field is further reduced (H_x = -100 mT). Since there is no antiferromagnetic exchange coupling between the layers, dipole coupling dominates the interaction, and therefore, the layers still prefer some degree of antiferromagnetic alignment. When, H_x = +20 mT (point 'c'), the layers are fully aligned antiferromagnetically, which is similar to the magnetization configurations for exchange-coupled nanomagnet in Fig. 1(b). Up to this point, the evolution of magnetization is not markedly different from the exchange-coupled nanomagnet with regard to the numerical value of M_y only, although the domain configurations of the layers are quite different due to their different coupling mechanisms. At H_x = +100 mT (point 'd'), we see that the top layer is turning toward the applied field, and the dipole coupling between the layers is now getting weaker and no longer holds the layers tightly antiferromagnetically aligned. The bottom layer has sizable end-domains, shown by the color contrast between the two ends and the center. At H_x = +160 mT (point 'e'), the top layer is now almost aligned to the field. However, the sizable end domains in the bottom layer disappear and a more uniform domain structure is observed. Beyond this point, M_y drops abruptly, unlike the exchange-coupled nanomagnets, as the horizontal field H_x tends to pull the magnetizations of the layers more to their hard axis. M_y crosses zero before reaching a minimum in the negative y direction. The magnetization snapshot at H_x = +200 mT (point 'f') is the situation when M_y reaches the minimum (M_y/M_s = -0.2). At this point, both layers tend to point to the direction of H_x, although not perfectly aligned to H_x. As H_x continues to increase, M_y starts increasing again and approaches zero. This behavior can be explained by the fact that there is always a vertical component of the field (H_y) present with H_x. From point 'f', the horizontal component (H_x) is strong enough to pull the net M_y toward the hard axis. At H_x = +400 mT (point 'g'), we see that the layers are fully biased along H_x.

For the dipole-coupled nanomagnets, the experimental data also agrees with the simulation – albeit not as precisely as in the case of exchange-coupled layers – while the curves look the same, the actual field values show quantitative differences. The M_y peaks around H_x = 20 mT – this simulation value is, however, not very accurate as we used a large (10 mT) field step in the OOMMF simulatons. The experimental value is 10 mT. At the peak, M_y/M_s = 0.51, which is close to the experimental value (M_y/M_s = 0.58). At the minimum, the simulated M_y/M_s = -0.2, which is also close to the experimental value (M_y/M_s = -0.28). M_y = 0, in this case, occurs at a field (H_x = 170 mT), which is significantly higher than that obtained from the experiment (H_x = 60 mT).

This major difference between the experimental and simulated data could be due to a variety of factors. In general, switching fields from nucleation/growth type processes are hard to predict. Since the switching here is the result of a nucleation/growth type process, and there is no exchange-coupling present between the layers to lock the magnetizations antiferromagnetically, process variations can contribute significantly to the deviation from the simulation. Lithographic variations can cause imperfections in the shape of the patterns,[17–19] and subsequent lift-off and ion-milling processes can roughen the nanomagnet edges and corners,[17] and also cause sidewall deposition[20] by the etch products. These effects can cause the magnets to switch along the hard axis at a lower field.[21–23] From a measurement viewpoint, averaging of the magnetization of millions of nanomagnets in the VSM can cause deviations from the behavior simulated from a single nanomagnet in OOMMF,[17] as it is extremely difficult to control uniformity over such a large array of nanomagnets and have a narrow switching distribution. Moreover, the simulation was performed at 0 K and for 1 ns at each field step, while the experiment was performed at room temperature and each field step was applied for a much longer time. It is not possible to perform the simulation within a longer time scale (seconds to hours), because it would make the process enormously computationally intensive.[24] At room temperature, the slower switching in the presence of thermal fluctuations can reduce the switching field, and thermal effects have more impact for nucleation-type switching processes.[25] Given all these possible sources of discrepancies, it can be said that the experimental data is well explained by the micromagnetic simulations in this case.

IV. CONCLUSION

We demonstrated the magnetization reversal process of nanomagnets patterned from the exchange- and dipole-coupled CoFe/Ru/CoFe multilayers. The measurements performed by the

vector coils of our VSM show distinct switching characteristics of the two types of structures. The experimental results are corroborated by the micromagnetic simulations, which reveal exchange-coupling-dominated macrospin-like switching in the exchange-coupled nanomagnets, and abrupt nucleation/growth type switching in the dipole-coupled nanomagnets. The simulations and experiments show an almost textbook-level illustration of the two distinct processes. Since exchange and dipole interactions are jointly present in most magnetoelectronic devices, our study contributes to a deeper understanding of the switching mechanisms in these devices.

ACKNOWLEDGMENTS

This work was supported by a grant from the U.S. NSF/SRC "Nanoelectronics for 2020 and Beyond" program. The authors thank Mr. Peng Li for his valuable inputs on the VSM measurement techniques.

[1] J. L. Costa-Krämer, J. Anguita, J. I. Martín, C. Martínez-Boubeta, A. Cebollada, and F. Briones, Nanotechnology **13**, 695–700 (2002).
[2] K. S. Buchanan, K. Y. Guslienko, A. Doran, A. Scholl, S. D. Bader, and V. Novosad, Phys. Rev. B **72**, 134415 (2005).
[3] H. Dey, G. Csaba, G. H. Bernstein, and W. Porod, Nanotechnology **27**, 395202 (2016).
[4] R. Lavrijsen, J. Lee, A. Fernández-Pacheco, D. Petit, R. Mansell, and R. P. Cowburn, Nature **493**, 647–650 (2013).
[5] L. Xu, H. Yu, M. S. Akhras, S. Han, S. Osterfeld, R. L. White, N. Pourmand, and S. X. Wang, Biosensors and Bioelectronics **24**, 99–103 (2008).
[6] F. J. Castano, Y. Hao, S. Haratani, C. A. Ross, B. Vogeli, M. Walsh, and H. I. Smith, IEEE Trans. Mag. **37**, 2073–2075 (2001).
[7] H. Dey, G. Csaba, F. Shah, G. H. Bernstein, and W. Porod, IEEE Trans. Mag. **52**, 4 (2016).
[8] V. S. Murthy, C. Krishnamoorthi, R. Mahendiran, and A. O. Adeyeye, J. Appl. Phys. **105**, 023916 (2009).
[9] C. A. Ross, F. J. Castano, E. Rodriguez, S. Haratani, B. Vogeli, and H. I. Smith, J. Appl. Phys. **97**, 053902 (2005).
[10] F. J. Castano, S. Haratani, Y. Hao, C. A. Ross, and H. I. Smith, Appl. Phys. Lett. **81**, 2809–2811 (2002).
[11] F. J. Castano, Y. Hao, S. Haratani, C. A. Ross, B. Vögeli, H. I. Smith, C. Sánchez-Hanke, C.-C. Kao, X. Zhu, and P. Grütter, J. Appl. Phys. **93**, 7927–7929 (2003).
[12] P. Li, Ph.D. thesis, University of Notre Dame, USA, 2014.
[13] P. Li, G. Csaba, V. K. Sankar, X. Ju, E. Varga, P. Lugli, X. S. Hu, M. Niemier, W. Porod, and G. H. Bernstein, IEEE Trans. Mag. **48**, 4402–4405 (2012).
[14] S. Reddy, J. J. Park, M. M. Maqableh, A. B. Flatau, and B. Stadler, J. Appl. Phys. **111**, 07A920 (2012).
[15] S. Parkin, Phys. Rev. Lett. **67**, 3598–3601 (1991).
[16] OOMMF software package, available online: http://math.nist.gov/oommf/.
[17] P. Li, G. Csaba, V. K. Sankar, X. Ju, P. Lugli, X. S. Hu, M. Niemier, W. Porod, and G. H. Bernstein, J. Appl. Phys. **111**, 07B911 (2012).
[18] M. Niemier, G. H. Bernstein, G. Csaba, A. Dingler, X. S. Hu, S. Kurtz, S. Liu *et al.*, J. Phys. Condens. Matter **23**, 493202 (2011).
[19] M. Niemier, M. Crocker, and X. S. Hu in *proceedings of the 23rd IEEE International Symposium on Defect and Fault Tolerance of VLSI Systems*, Boston, USA, Oct. 1-Oct. 3, 2008, edited by C. Bolchini, Y. Kim, D. Gizopoulos, and M. Tehranipoor (IEEE Computer Society, Los Alamitos, 2008), pp. 534–542.
[20] F. Shah, Ph.D. thesis, University of Notre Dame, USA, 2015.
[21] R. P. Cowburn, D. K. Koltsov, A. O. Adeyeye, and M. E. Welland, J. Appl. Phys. **87**, 7067–7069 (2000).
[22] J. Gadbois, J. Zhu, W. Vavra, and A. Hurst, IEEE Trans. Mag. **34**, 1066–1068 (1998).
[23] Y. Nakatani, A. Thiaville, and J. Miltat, Nat. Mater. **2**, 521–523 (2003).
[24] G. Csaba and W. Porod, in *proceedings of the 14th International Workshop on Computational Electronics (IWCE)*, Pisa, Italy, Oct. 27-Oct. 29, 2010, pp. 1–4.
[25] M. P. Sharrock, J. Appl. Phys. **76**, 6413–6418 (1994).